SUPPORTING INFORMATION

Global Dynamics and Exchange Kinetics of a Protein on the Surface of Nanoparticles Revealed by Relaxation-Based Solution NMR Spectroscopy

Alberto Ceccon, Vitali Tugarinov*, Ad Bax and G. Marius Clore*

Laboratory of Chemical Physics, National Institute of Diabetes and Digestive and Kidney Diseases, National Institutes of Health, Bethesda, Maryland 20892-0520, U. S. A.

Materials and Methods

Preparation of NMR samples.

Recombinant Ubiquitin was expressed and purified as described previously.[S1] Ubiquitin samples with two labeling schemes were used in the current work: U-[^{15}N/^{2}H]-labeled ubiquitin), and [^{2}H/^{15}N/Ileδ_1-$^{13}CH_3$/Leu,Val-$^{13}CH_3$/$^{12}CD_3$]-labeled ubiquitin. Note that only one of the two methyl groups of the isopropyl moieties of Val and Leu is ^{13}C-labeled and protonated.[S2,S3] All NMR samples were prepared in 10 mM phosphate buffer (K_2HPO_4/KH_2PO_4), pH 6.8, and 7% D_2O/93% H_2O. The final concentration of ubiquitin upon addition of the liposome solution (see below) was kept between 0.8 mM and 0.9 mM.

Preparation of liposome solutions.

The sodium salt of 1-palmitoyl-2-oleoyl-*sn*-glycero-3-phospho-(1'-*rac*-glycerol) (POPG), 1-palmitoyl-2-oleoyl-*sn*-glycero-3-phosphocholine (POPC), and the gadolinium salt of 1,2-distearoyl-*sn*-glycero-3-phosphoethanolamine-N-diethylenetriaminepentaacetic acid (18:0 PE-DTPA-Gd^{3+}) were purchased from Avanti Polar Lipids (Alabaster, AL). Diamagnetic large unilamellar vesicles (LUVs)

were prepared by dissolving an aliquot of POPG or POPC phospholipids and 20% (mol/mol) cholesterol into a round-bottom flask. For preparation of paramagnetic LUVs, 10% (mol/mol) of 18:0 PE-DTPA-Gd^{3+} phospholipid was added to the lipid mixture. The solvent was then removed and the lipid suspension dried by slow evaporation under nitrogen flux. Re-suspension of the film was carried out in 10 mM phosphate buffer (K_2HPO_4/KH_2PO_4), pH 6.8 to a final lipid stock concentration of 5 mM. Complete hydration of the dried film was accomplished by keeping the lipid suspension above the transition temperature (T_m) for 12 hrs. Homogenous LUVs were obtained by repeatedly extruding the lipid suspension through polycarbonate filters (1 μm, 400 nm, 100 nm) to obtain uniformly sized unilamellar vesicles of ~100 nm in diameter. Small unilamellar vesicles (SUV) were prepared via sonication without cooling at 15 Watt for 20 min using probe tip sonicator (Misonix, NY). After sonication, SUV solutions were centrifuged to sediment small bits of metal released by the sonication tip. Liposome solutions were stored in the dark at room temperature to prevent lipid oxidation.

Dynamic light scattering.

The particle size distribution and ζ-potential of the LUV and SUV vesicles were determined by dynamic light scattering (DLS) at 25°C upon dilution of the samples to 0.5 mM (in lipid) with 10 mM phosphate buffer (pH 6.8) and to 1 mM (in lipid) with high purity water, respectively. Measurements were performed using the Zetasizer Nano ZS (Malvern Instruments, US) instrument operating at a wavelength of $\lambda = 633$ nm. Reducing the conductivity of the sample to less than 1 mS/cm improved the quality of the phase plot and reproducibility of the data. The measurements of size and ζ-potential were repeated 5 times after a 2 min temperature equilibration. The ζ-potential of lipid-based POPG vesicles was calculated from the electrophoretic mobility via the Helmholtz-Smoluchowski equation.[S4] To be considered significant the number of sub-runs for each measurement was increased to reach mean count rates between 100 and 200 kcps.

NMR spectroscopy.

All NMR experiments were recorded at 25°C using Bruker Avance-III spectrometers, equipped with Bruker TCI triple resonance *z*-axis gradient cryogenic probes, at ^1H Larmor frequencies of 800.13, 700.24, and 500.68 MHz. All experiments were performed on 0.8-0.9 mM ubiquitin dissolved in 10 mM phosphate buffer (pH 6.8), 7% D_2O/93% H_2O (v/v). For PRE measurements, experiments were carried out using diamagnetic and paramagnetic POPG vesicles with a protein/lipid ratio of 1:2 (mol/mol).

^{15}N, ^{1}H$_{N}$, and ^{1}H$_{methyl}$ transverse relaxation rate measurements.

^{15}N $R_{1\rho}$ and R_1 values were measured using pulse schemes described previously.[S9,10] Experiments were performed on free ubiquitin and ubiquitin in the presence of LUVs at 800, 700 and 500 MHz; measurements in the presence of SUVs were carried out at 800 and 500 MHz. Typically, a spin-lock field strength of 1.8 kHz was employed with spin-lock periods of 1, 15, 30, 40, 60 and 80 ms to suppress chemical exchange (R_{ex}) contributions to ^{15}N relaxation rates. ^{15}N-R_1 measurements were performed using delays of 40, 120, 200, 280, 400 and 480 ms. ^{15}N-R_2 values were extracted from the measured $R_{1\rho}$ and R_1 rates using the following relationship:

$$R_2 = (R_{1\rho} - R_1 \cos^2\theta)/\sin^2\theta, \quad \text{(S1)}$$

where θ is the angle subtended by the effective spin-lock field with respect to the external magnetic field (and 90° represents a resonance exactly on-resonance with the spin-lock field).

Free-precession ^{1}H$_{N}$-R_2 relaxation rates of ubiquitin in the presence of LUV liposomes were measured using standard procedures.[S6] Relaxation delays of 1, 5, 10, 20, 30, 40, 60 and 80 ms were applied for diamagnetic samples, while delays of 1, 2, 4, 6, 8, 10, 12, 15, 17 and 20 ms were used for paramagnetic samples. Free-precession R_2 relaxation rates of methyl protons (^{1}H$_{methyl}$-R_2) were measured using a pulse scheme that selects for the slowly relaxing ^{1}H transitions in ^{13}CH$_3$ methyl groups as described earlier.[S2] Relaxation delays of 20, 40, 80, 120, 160, 200, 240 and 280 ms were used for diamagnetic samples, and delays of 2, 4, 6, 8, 10, 12 and 16 ms were used for paramagnetic samples.

Lifetime line-broadening (ΔR_2) values were calculated as the differences between ^{15}N, ^{1}H$_{N}$, or ^{1}H$_{methyl}$ R_2 values obtained in the presence of LUV or SUV vesicles and those obtained for free ubiquitin. Intermolecular transverse PRE rates (Γ_2) for ^{1}H$_{N}$ and ^{1}H$_{methyl}$ nuclei were obtained from the difference between the measured R_2 rates in the presence of paramagnetic and diamagnetic LUVs.

2D ^{1}H$_{N}$-DEST measurements[S6] were performed at 700 MHz with a ^{1}H$_{N}$ saturation period preceding the [^{1}H-^{15}N]-HSQC 'read-out' scheme. Continuous wave (CW) saturation was applied at radiofrequency (RF) field strengths of 350 and 180 Hz for 1.0 s at the following offsets from the carrier frequency (in kHz): 2.0, 3.0, 3.5, 4.0, 4.5, 5.0, 5.5, 6.0, 6.5, 7.0, 7.5, 8.0, 9.0, 10.0, 12.0, 14.0 and 18.0. The carrier was set to 119.5 ppm for ^{15}N and 4.7 ppm for ^{1}H. Control experiments were performed with the CW saturation turned off and the highest positive offset values. A total of 80*x850* complex data points were acquired in the indirect (^{15}N) and direct (^{1}H$_{N}$) dimensions, respectively, with respective acquisition times of 45 and 87 ms resulting in the total measurement time of 84 min. per 2D experiment. ^{1}H$_{methyl}$ DEST experiments were recorded at 700 MHz. The implementation of ^{1}H$_{methyl}$-DEST involved a saturation period appended

to the beginning of an HMQC-based pulse scheme that selects for the slowly relaxing ^{1}H transitions in $^{13}CH_3$ methyl groups as described in detail elsewhere.[S8] Saturation RF field strengths of 350 and 180 Hz were for applied 1.0 s at the following offsets from the carrier (in kHz): -10.0, -8.0, -6.0, -5.0, -4.0, -3.0, -2.5, -2.0, -1.5, -1.0, -0.5, -0.3, 0.0, 0.3, 0.5, 1.0, 1.5, 2.0, 2.5, 3.0, 4.0, 5.0, 6.0, 8.0 and 10.0. A total of 128* x 512* complex data points were acquired in the indirect ($^{13}C_{methyl}$) and direct ($^{1}H_{methyl}$) dimensions with respective acquisition times of 36 and 73 ms resulting in the total measurement time of 70 min. per 2D experiment.

Analysis of lifetime line broadening (ΔR_2) data of ubiquitin in the presence of LUV and SUV nanoparticles.

Generally, the broadening of NMR lines of a protein in the presence of LUV or SUV nanoparticles (ΔR_2) can be calculated from the solution of a set of McConnell equations[S11,12] as described in detail in our previous publications.[S9,10] In the present work, the coupled evolution of the transverse magnetization of the free state of ubiquitin (A) and its LUV/SUV-bound state (B) was modeled using a simplified variant of the McConnell equations for a two-site exchange system, assuming the absence of chemical shift differences between the two states:

$$\frac{d}{dt}\begin{bmatrix} I^{\mathrm{A}} \\ I^{\mathrm{B}} \end{bmatrix} = -\begin{bmatrix} R_2^{\mathrm{A}} + k_{\mathrm{on}}^{\mathrm{app}} & -k_{\mathrm{off}} \\ -k_{\mathrm{on}}^{\mathrm{app}} & R_2^{\mathrm{B}} + k_{\mathrm{off}} \end{bmatrix}\begin{bmatrix} I^{\mathrm{A}} \\ I^{\mathrm{B}} \end{bmatrix} \qquad \text{(S2)}$$

where I^{A} and I^{B} are the transverse magnetizations of states A and B, respectively, $k_{\mathrm{on}}^{\mathrm{app}}$ is the apparent association rate constant, k_{off} is the dissociation rate constant, and R_2^{A} and R_2^{B} are the intrinsic transverse relaxation rates in the free (A) and bound (B) states, respectively (in the absence of exchange). Although the system of differential equations in Eq. (S2) has a closed-form analytical solution - *e.g.* for initial conditions $\{I^{\mathrm{A}}(0) = p_{\mathrm{A}}; I^{\mathrm{B}}(0) = p_{\mathrm{B}}\}$ the time evolution of I^{A} is given by,

$$I^{\mathrm{A}}(t) = p_{\mathrm{A}} exp[-(R_2^A + R_2^B + k_{\mathrm{off}} + k_{\mathrm{on}}^{\mathrm{app}})t/2]\{cosh(\eta t) + [(R_2^B - R_2^A + k_{\mathrm{off}} - k_{\mathrm{on}}^{\mathrm{app}})/2\eta]sinh(\eta t)\} + p_B(k_{\mathrm{off}}/\eta)exp[-(R_2^A + R_2^B + k_{\mathrm{off}} + k_{\mathrm{on}}^{\mathrm{app}})t/2]sinh(\eta t) \qquad \text{(S3)}$$

where $\eta = (1/2)[(R_2^{\mathrm{A}} + k_{\mathrm{on}}^{\mathrm{app}})^2 + (R_2^{\mathrm{B}} + k_{\mathrm{off}})^2 - 2(R_2^{\mathrm{A}} + k_{\mathrm{on}}^{\mathrm{app}})(R_2^{\mathrm{B}} + k_{\mathrm{off}}) + 4k_{\mathrm{on}}^{\mathrm{app}} k_{\mathrm{off}}]^{1/2}$; and p_{A} and p_{B} are the equilibrium populations of the two states (p_B = 1 - p_A = $k_{\mathrm{on}}^{\mathrm{app}} / k_{\mathrm{ex}}$, p_A = $k_{\mathrm{off}} / k_{\mathrm{ex}}$, and $k_{\mathrm{ex}} = k_{\mathrm{on}}^{\mathrm{app}} + k_{\mathrm{off}}$) - the latter solution is of little practical utility in the present case owing to the very large values of k_{ex} and R_2^B.

ΔR_2 values can be evaluated from the time evolution of I^{A} in Eqs. (S2) and (S3) as:[S5]

$$\Delta R_2 = \ln[I^{\mathrm{A}}(\tau_1) / I^{\mathrm{A}}(\tau_2)] / (\tau_2 - \tau_1) \tag{S4}$$

where the delays τ_1 and τ_2 are chosen to remove any deviations from single-exponential behavior at very short delays, and to match the order of magnitude of the experimental decay, respectively. Typically, τ_1 = and τ_2 delays of 10 and 70 ms, respectively, were used for LUV ^{15}N-ΔR_2, 10 and 30 ms for SUV ^{15}N-ΔR_2, 10 and 70 ms for diamagnetic LUV ^{1}H$_{\mathrm{N}}$-ΔR_2, and 5 and 15 ms for paramagnetic LUV ^{1}H$_{\mathrm{N}}$-ΔR_2. Note that in the limit of very fast exchange ($k_{\mathrm{ex}} >> R_2^{\mathrm{B}} - R_2^{\mathrm{A}}$), the evolution of I^{A} can, to a very good approximation, be described by a single-exponential decay with $R_2^{\mathrm{B}} \sim \Delta R_2 / p_{\mathrm{B}}$. Outside of this limit, however, this simple expression for R_2^B leads to *underestimation* of the R_2 rates in the bound state.

In our previous publications,[S5-S7,S8,S9] the transverse relaxation rates in the bound ('dark') state(s) R_2^B were treated phenomenologically, in the sense that they were allowed to vary freely during minimization of an error function comparing experimental and calculated data, and were not quantitatively interpreted in the framework of a motional model. In the present study, the large variability of the measured ΔR_2 values (Figs. 1A and B in the main text) necessitated the adoption of a different approach in which the fitted R_2^B values were calculated using available theoretical expressions for ^{15}N/^{1}H$_{\mathrm{N}}$ transverse relaxation[S13] in the framework of a simple model of global protein dynamics.

R_2 values are related to molecular dynamics through their dependence on linear combinations of the power spectrum of the motion (or 'spectral density function') at a finite number of frequencies ω (*e.g.* for a ^{15}N nucleus coupled to a proton - at 0, ω_{N}, ω_{H}, $\omega_{\mathrm{H}} + \omega_{\mathrm{N}}$, and $\omega_{\mathrm{H}} - \omega_N$, where ω_i is the Larmor frequency of nucleus *i*):[S13]

$$\begin{aligned} {}^{15}\mathrm{N}\text{-}R_2 = {} & 0.05(\gamma_{\mathrm{H}}\gamma_{\mathrm{N}}\hbar < r_{\mathrm{HN}}^{-3} >)^2 [4J(0) + J(\omega_{\mathrm{H}} - \omega_{\mathrm{N}}) + 3J(\omega_{\mathrm{N}}) + 6J(\omega_{\mathrm{H}}) + 6J(\omega_{\mathrm{H}} + \omega_{\mathrm{N}})] \\ & + (1/45)\omega_{\mathrm{N}}^2(\sigma_{\parallel} - \sigma_{\perp})(3J(\omega_{\mathrm{N}}) + 4J(0)] \end{aligned} \tag{S5}$$

where γ_{H} and γ_{N} are the gyromagnetic ratios of ^{1}H and ^{15}N nuclei, respectively; $\hbar$ is Planck's constant divided by 2π; r_{HN} is the N-H bond length (1.02 Å); and $(\sigma_{\parallel} - \sigma_{\perp})$ is the ^{15}N chemical shift anisotropy (-170 ppm), where $\sigma_{\parallel}$ and $\sigma_{\perp}$ are the parallel and perpendicular components of the axially symmetric ^{15}N chemical shift tensor.

The simplest approach that relates the spectral density function to motional parameters is the model-free[S14] and extended model-free[S15,S16] formalism in which values of squared order parameters (S^2) and time-scales of various motions (τ) are extracted to characterize the details of molecular dynamics. The extended model-free formulation[S15,S16] of the spectral density function $J(\omega)$, used here to describe the global dynamics of ubiquitin on the surface of LUV and SUV nanoparticles, is given by:

$$J(\omega) = S_{\mathrm{w}}^2[P_2(\cos\alpha)]^2 \frac{\tau_{\mathrm{C}}}{1+(\omega\tau_{\mathrm{C}})^2} + S_w^2(1-[P_2(\cos\alpha)]^2)\frac{\tau'_{\mathrm{r}}}{1+(\omega\tau'_{\mathrm{r}})^2} + (1-S_{\mathrm{w}}^2)\frac{\tau'_{\mathrm{w}}}{1+(\omega\tau'_{\mathrm{w}})^2} \qquad \text{(S6)}$$

where the second order Legendre polynomial $P_2(\cos\alpha) = (3\cos^2\alpha - 1)/2$ represents the order parameter S_{r} (in the main text) for axially symmetric internal rotation around an axis forming an angle α with the direction of an N-H bond vector; S_{w} is the order parameter of the wobbling motion occuring in a cone centered about the internal rotation axis (see Fig. 2B in the main text); τ_{C} is the total effective correlational time; and τ'_{r} and τ'_{w} are effective correlation times for internal rotation and wobbling. The various effective correlation times are given by:

$$\tau_{\mathrm{C}} = \tau_{\mathrm{R}}\tau_{\mathrm{ex}}/(\tau_{\mathrm{R}}+\tau_{\mathrm{ex}}); \quad \tau'_{\mathrm{r}} = \tau_{\mathrm{r}}\tau_{\mathrm{C}}/(\tau_{\mathrm{r}}+\tau_{\mathrm{C}}); \quad \tau'_{\mathrm{w}} = \tau_{\mathrm{w}}\tau_{\mathrm{C}}/(\tau_{\mathrm{w}}+\tau_{\mathrm{C}}) \qquad \text{(S7)}$$

where τ_{R} is the rotational correlation time of molecular tumbling of the nanoparticle, $\tau_{\mathrm{ex}} = (k_{\mathrm{on}}^{\mathrm{app}} + k_{\mathrm{off}})^{-1}$ is the lifetime (or residence time) of bound ubiquitin, and τ_{r} and τ_{w} are the internal rotation and wobbling correlation times, respectively, for ubiquitin on the surface of the nanoparticle. The formulation in Eq. (S6) requires that the time scales of motion can be separated with $\tau_{\mathrm{C}} > \tau_{\mathrm{r}} > \tau_{\mathrm{w}}$. In calculating R_2 from $J(\omega)$ (ref. S13), values of 1.02 Å and -170 ppm were employed for the N-H bond length and ^{15}N chemical shift anisotropy, respectively. The values of τ_{R} for LUVs and SUVs were estimated to be 100 and 1.8 μs, respectively, calculated from the corresponding particle diameters (103 and 27 nm, respectively; cf. Fig. S1) using the Stokes-Einstein equation.

The small but clear dependence of experimental ^{15}N-ΔR_2 values on static magnetic field strength (see Figs. 1C and D of the main text and Fig. S2) implies that $k_{\mathrm{ex}} > R_2^{\mathrm{B}} - R_2^{\mathrm{A}}$ (the detailed analysis of ubiquitin binding, *vide infra*, yields a value of $k_{\mathrm{ex}} \sim 50{,}000\ \mathrm{s}^{-1}$). In this regime, exchange is fast on the relaxation time-scale making the problem of characterizing the binding equilibrium (i.e. extraction of values for $k_{\mathrm{on}}^{\mathrm{app}}$ and k_{off} without assumptions about either of them) ill-determined for both LUV and SUV binding, irrespective of whether the R_2^B rates are treated phenomenologically or calculated using the spectral density in Eqs. (S6) and (S7). Indeed, the ^{15}N-ΔR_2 data for ubiquitin in the presence of LUVs and SUVs can be fitted with a continuum of $\{k_{\mathrm{on}}^{\mathrm{app}}; k_{\mathrm{off}}; R_2^B\}$ sets of solutions once $\Delta R_2 \approx p_{\mathrm{B}} R_2^{\mathrm{B}} \approx (k_{\mathrm{on}}^{\mathrm{app}}/k_{\mathrm{off}})R_2^{\mathrm{B}}$.

Further, practically no new information is provided by ^{15}N-DEST experiments in this exchange regime - for example, the simulated ^{15}N-DEST profiles for ubiquitin-LUV binding are almost indistinguishable from the profiles obtained for the free protein. This ill-determinacy is not alleviated when the R_2^B values are modelled according to the extended model-free spectral density in Eq. (S6), as the R_2^B values are themselves dependent on the time-scale of exchange through the value of τ_C in the first terms of Eqs. (S6) and (S7).

The resolution of the uncertainties described above lies in the *combined* use of the ^{15}N-ΔR_2 data obtained in the presence of vesicles of varying sizes (LUVs and SUVs) on the reasonable assumption that the global motional parameters and dissociation rate constant are independent of particle size. Specifically, we require that the time-scale of internal rotation τ_r, the polar angles $(\theta;\varphi)$ that describe the orientation of the internal rotation axis in the molecular inertia frame, the parameters of the wobbling motion (S_w and τ_w), and the dissociation rate constant k_{off} are the same for ubiquitin binding to LUV and SUV particles. This drives the otherwise very large parameter space to a relatively well-defined minimum, as a consequence of very different relative contributions of the rotational tumbling time τ_R and k_{off} to the effective total correlation time τ_C (Eq. S7) for LUVs and SUVs: τ_R contributes less than 10 % to τ_C for LUVs but >90% to τ_C for SUVs. As a result, τ_C of SUVs is smaller than that of LUVs by about an order of magnitude, and the effects of internal rotation and wobbling on the observed ΔR_2 rates in the smaller SUV vesicles are concomitantly less pronounced leading to much smaller variability of ΔR_2 in SUVs (*cf.* Figs. 1A and B in the main text, and Fig. S2).

The restraining of parameter space by simultaneous use of LUV and SUV ΔR_2 data, under the assumptions described above, is illustrated in Fig. S3 which shows plots of τ_r values (ns) versus chosen (fixed in the fit) k_{off} values (s^{-1}) obtained from separate fits of LUV (shown in blue) and SUV (shown in red) ^{15}N-ΔR_2 data for a number of (S_w^2; τ_w) parameter sets (also fixed in the fit). The points where the LUV (blue) and SUV (green) curves intersect (connected by the red curves in Fig. S3) indicate possible solutions that would satisfy both LUV and SUV ^{15}N-ΔR_2 data simultaneously. It is clear from Fig. S3 that possible values of S_w^2 cover a range between ~0.2 and ~0.7. If the value of S_w^2 is low (< 0.4), however, then the time-scale for wobbling, τ_w, cannot be higher than ~500 ns since the resulting values of τ_r will otherwise approach the same time-scale as that of wobbling (Fig. S3). All the kinetic and dynamics parameters reported in the main text for ubiquitin binding to LUV and SUV liposomes are obtained with S_w^2 and τ_w fixed at respective values of 0.5 and 300 ns. The values of the kinetic and dynamics parameters remain within their reported uncertainties for S_w^2 in the range between 0.2 and 0.7 as long as τ_w does not exceed a value of ~500 ns.

It has not escaped our attention that if wobbling were to occur on a time-scale *slower* than internal rotation, a reformulation of the spectral density function would be in order involving the swapping of the squared order parameters S_w^2 and $[P_2(\cos\alpha)]^2$ (S_r^2) and the correlation times τ_w' and τ_r' in Eq. (S6).

However, the fits to the LUV and SUV ^{15}N-ΔR_2 values using this re-formulated spectral density consistently resulted in reduced χ^2 values that are more than a factor of 3 higher than when Eq. (S6) is used, indicating that the $[P_2(\cos\alpha)]^2$-dependence of the calculated ΔR_2 on the angle α is in better agreement with experimental data when attributed *only* to slower motions.

For combined analysis of LUV and SUV ^{15}N-ΔR_2 data, the following error function F was minimized in the non-linear least squares fitting procedure:

$$F = \alpha_1 \sum_i \sum_{j=1}^{3} \left(\frac{\Delta R_{2,\mathrm{LUV}}^{\mathrm{obs},i,j} - \Delta R_{2,\mathrm{LUV}}^{\mathrm{calc},i,j}}{\sigma_{\Delta R_{2,\mathrm{LUV}}}^{i,j}} \right)^2 + \alpha_2 \sum_i \sum_{j=1}^{2} \left(\frac{\Delta R_{2,\mathrm{SUV}}^{\mathrm{obs},i,j} - \Delta R_{2,\mathrm{SUV}}^{\mathrm{calc},i,j}}{\sigma_{\Delta R_{2,\mathrm{SUV}}}^{i,j}} \right)^2 \qquad \text{(S8)}$$

where the subscripts i and j refer to residue number (a total of 59 residues were analyzed) and spectrometer field strength (500, 700 and 800 MHz for LUVs, and 500 and 800 MHz for SUVs), respectively, and $\sigma_{\Delta R}$ represents the standard error of the measurement. $\Delta R_2^{\mathrm{calc}}$ in Eq. (S8) was calculated using Eqs. (S2) and (S4), where the rates R_2^{B} are calculated using the form of the spectral density in Eqs. (S6) and (S7). (Note that the data for residues displaying a high degree of local dynamics in free ubiquitin, specifically residues 8 and 9 in a flexible loop and residues 72-76 in the disordered C-terminal tail, were omitted from analysis.) The set of global variable parameters of the fit comprised $\{k_{\mathrm{on}}^{\mathrm{app,LUV}}; k_{\mathrm{on}}^{\mathrm{app,SUV}}; k_{\mathrm{off}}; \tau_{\mathrm{r}}; \theta; \varphi\}$, where θ and φ are the polar angles that define the orientation of the rotation axis in the frame of the inertia tensor of ubiquitin (see Fig. 2), and α_1 and α_2 are the scaling factors that define the relative contribution of LUV and SUV data to the total error function. The uncertainties in the values of the optimized parameters, corresponding to confidence intervals of ±1 S.D., were determined from the variance-covariance matrix of the non-linear fit. The minimization of F was performed with several different combinations of factors α yielding parameters of global motion largely within their respective uncertainties. Throughout this work, we report the values obtained with $\alpha_1 = \alpha_2 = 1$ in Eq. (S8) as this still ensures a slightly higher weight assigned to the LUV data (where the variability in ΔR_2 is much higher) as the latter were acquired at three spectrometer fields as opposed to only two for SUVs. Convergence of the solution was confirmed by varying initial values for all parameters and obtaining the same solution within reported errors. The error function for the fitting ^{1}H$_{\mathrm{N}}$-ΔR_2 values (Fig. S4C) included only the first (LUV) term of Eq. (S8) at a single spectrometer field (700 MHz) and was performed with k_{off} and τ_{r} fixed at the values obtained from analysis of the ^{15}N-ΔR_2 data using the set of optimized parameters that included $\{k_{\mathrm{on}}^{\mathrm{app}}; \theta; \varphi\}$. The ^{1}H$_{\mathrm{N}}$-derived values of $k_{\mathrm{on}}^{\mathrm{app}}$ and the polar angles θ and φ were within the range of uncertainties of ^{15}N-ΔR_2-derived parameter values.

Estimation of diffusion limited association rate constants for the binding of ubiquitin to nanoparticles.

Ubiquitin can bind anywhere on the surface of the nanoparticle (i.e. binding is non-specific). The diffusion limited association rate constants for non-specific binding of ubiquitin to LUV and SUV nanoparticles was estimated from the Smoluchowski equation,[S17] $4\pi D_{trans}RN/1000$, where D_{trans} is the translation diffusion constant of ubiquitin, 1.2×10^{6} cm^2s^{-1} at 300K;[S18] R the nanoparticle radius; and N, Avogadro's number.

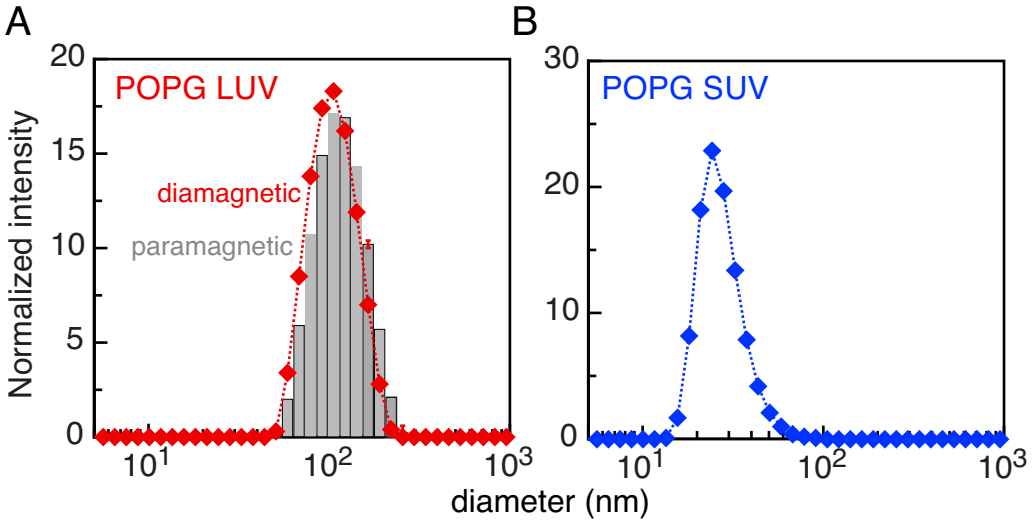

Figure S1. Characterization of POPG LUV and SUV nanoparticles by dynamic light scattering (DLS). (**A**) Particle size distribution of 0.5 mM (in lipid molecules) diamagnetic (red diamonds) and paramagnetic (grey bars) POPG LUVs. The size distribution for diamagnetic and paramagnetic LUVs is 103±1 and 108±1 nm, respectively. (**B**) Particle size distribution of 0.5 mM (in lipid molecules) diamagnetic (blue diamonds) POPG SUVs. The size distribution for POPG SUVs is 27±2 nm. The polydispersity index (PDI) for POPG LUVs and SUVs is less than 0.1 and 0.2, respectively. LUVs and SUVs were stable for more than a week, and had a ζ-potential of about -55 mV indicative of a stable particle suspension.[S19]

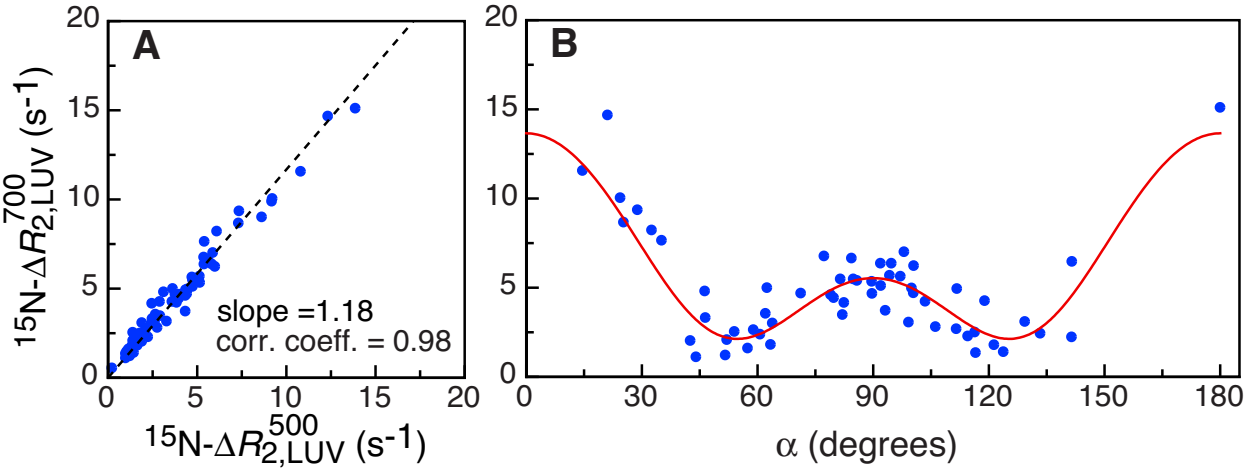

Figure S2. ^{15}N-ΔR_2 measurements on U-[^{15}N/^{2}H] ubiquitin dissolved in H_2O in the presence of LUVs. (**A**) Correlation plot of ^{15}N-ΔR_2 values measured at 700 and 500 MHz. The black dashed line is the simulated correlation derived from the simultaneous best-fitting of all the LUV and SUV data. The average ratio of ^{15}N-ΔR_2 values at 700 to 500 MHz is 1.18, comparable to the expected ratio of 1.20 from a relaxation mechanism based on the one-bond ^{1}H-^{15}N dipolar interaction and a -170 ppm ^{15}N chemical shift anisotropy. **(B)** Dependence of ^{15}N-ΔR_2 values measured at 700 MHz on the angle α between the N-H bond vectors and the internal rotation axis. Experimental data is shown as blue circles, and the best-fit curve obtained from global fits (with S_w^2 and τ_w fixed at 0.5 and 300 ns, respectively) is shown with a solid red line. Data for residues displaying a high degree of local dynamics in free ubiquitin, specifically residues 8 and 9 in a flexible loop and residues 72-76 in the disordered C-terminal tail, were omitted from analysis. The concentration of ubiquitin is 0.8 mM with a 1:2 ratio (mol/mol of a lipid molecule basis) of POPG LUVs. The data were collected at 25°C.

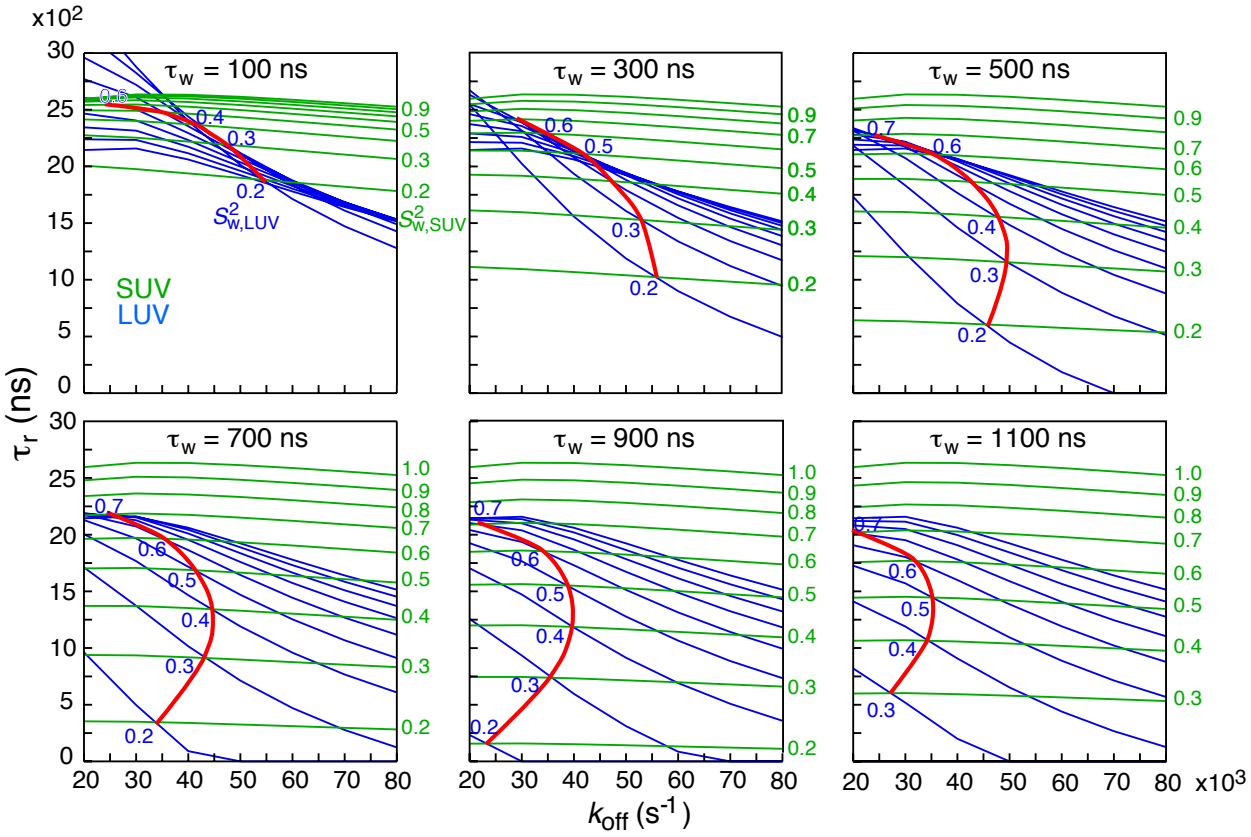

Figure S3. Grid search showing the dependence of the internal rotation correlation time (τ_r) on the dissociation rate constant k_{off} obtained from separate fits to LUV (blue lines) and SUV (green lines) ^{15}N-ΔR_2 data for a range of k_{off} (x-axis), S_w^2 (labeled on the figures) and τ_w (indicated on top of each panel) sets of parameters. The points where the LUV and SUV curves intersect (connected with the red curves) indicate possible solutions (τ_r and k_{off} values) that satisfy both the LUV and SUV data simultaneously.

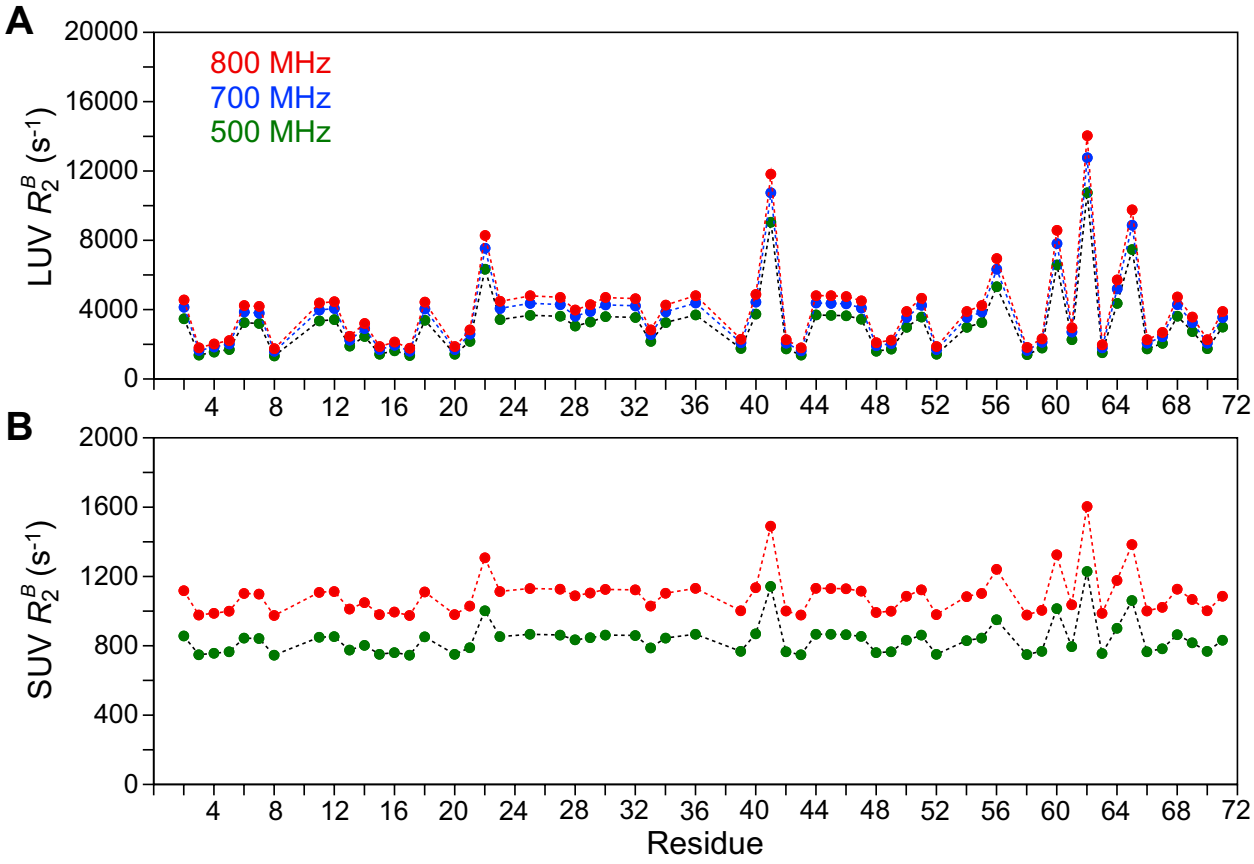

Figure S4. Calculated transverse relaxation rates of ubiquitin bound to liposome nanoparticles. R_2^B profiles for ubiquitin bound to (**A**) LUVs and (**B**) SUVs at several spectrometer fields calculated using the optimized parameters of exchange and dynamics (see main text and Fig. 2 of main text).

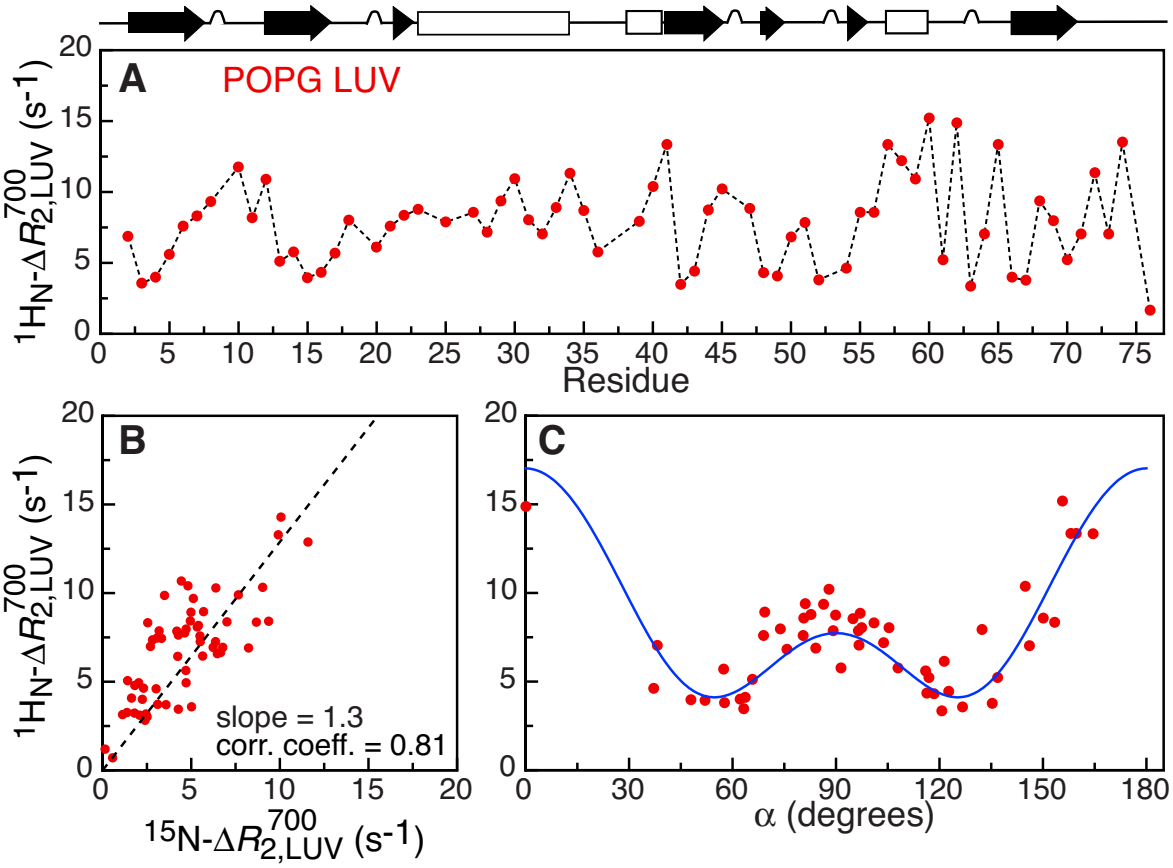

Figure S5. Experimental ^1H_N-ΔR_2 measurements on U-[$^{15}N/^2H$] ubiquitin dissolved in H_2O in the presence of LUVs. **(A)** Experimental ^1H_N-ΔR_2 profile measured for 0.8 mM ubiquitin in the presence of a 1:2 ratio (mol/mol on a lipid molecule basis) negatively charged POPG LUVs at 700 MHz. **(B)** Correlation plot comparing ^{15}N- and ^1H_N-ΔR_2 at 700 MHz; **(C)** Dependence of ^1H_N-ΔR_2 values on the angle α between the H-N bond vectors and the internal rotation axis with experimental data points shown as blue circles and the best-fit curve (with S_w^2 and τ_w fixed at 0.5 and 300 ns, respectively) displayed as a red line. Data for residues displaying a high degree of local dynamics in free ubiquitin, specifically residues 8 and 9 in a flexible loop and residues 72-76 in the disordered C-terminal tail, were omitted from analysis. In addition, data for residues 8, 12, 30, 34, 35, 58 and 59 were omitted owing to contamination from ^1H-^1H dipolar interactions. The ubiquitin coordinates used in the analysis are taken from the X-ray structure (PDB 1UBQ)[S20] with protons added using Xplor-NIH.[S21] A schematic diagram of the secondary structure of ubiquitin is shown on top of panel A.

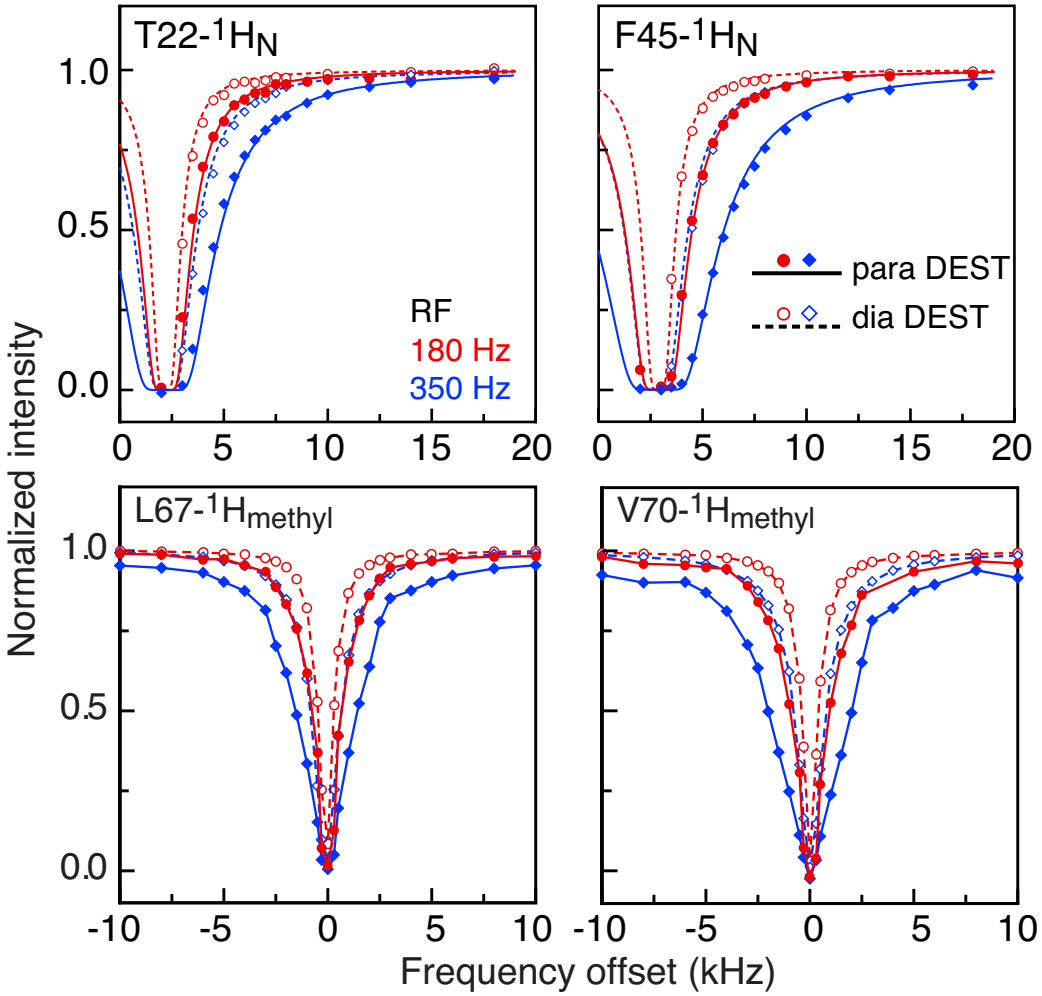

Figure S6. Examples of ^1H_N and $^1H_{methyl}$ DEST profiles measured for ubiquitin in the presence of a 1:2 ratio (on a lipid molecule basis) diamagnetic and paramagnetic (Gd^{3+}-tagged) LUV nanoparticles. DEST profiles were acquired at two different continuous wave radiofrequency (RF) field strengths as indicated in the figure. Data obtained for diamagnetic and paramagnetic LUVs are indicated by open and filled-in symbols, respectively, connected by dashed and continuous lines to guide the eye. Note the wider DEST profiles in the presence of Gd^{3+}-tagged LUVs. Only the downfield portion of the ^1H_N-DEST profiles are shown to exclude artefacts introduced by saturation of the water resonance.

Supplementary references

(S1) Varadan, R.; Assfalg, M.; Haririnia, A.; Raasi, S.; Pickart, C.; Fushman, D. *J. Biol. Chem.* **2004**, *279*, 7055-7063.

(S2) Tugarinov, V.; Kanelis, V.; Kay, L. E. *Nat Protoc* **2006**, *1*, 749-754.

(S3) Tugarinov, V.; Kay, L. E. *J. Biomol. NMR* **2004**, *28*, 165-172.

(S4) Egorova, E. M. *Electrophoresis* **1994**, *15*, 1125-1131.

(S5) Fawzi, N. L.; Ying, J. F.; Ghirlando, R.; Torchia, D. A.; Clore, G. M. *Nature* **2011**, *480*, 268-271.

(S6) Fawzi, N. L.; Ying, J. F.; Torchia, D. A.; Clore, G. M. *J. Am. Chem. Soc.* **2010**, *132*, 9948-9951.

(S7) Fawzi, N. L.; Libich, D. S.; Ying, J. F.; Tugarinov, V.; Clore, G. M. *Angew Chem Int Edit* **2014**, *53*, 10345-10349.

(S8) Tugarinov, V.; Kay, L. E. *J. Am. Chem. Soc.* **2006**, *128*, 7299-7308.

(S9) Libich, D. S.; Fawzi, N. L.; Ying, J.; Clore, G. M. *Proc. Natl. Acad. Sci. U. S. A.* **2013**, *110*, 11361-11366.

(S10) Libich, D. S.; Tugarinov, V.; Clore, G. M. *Proc. Natl. Acad. Sci. U. S. A.* **2015**, *112*, 8817-8823.

(S11) McConnell, H. M. *J. Chem. Phys.* **1958**, *28*, 430-431.

(S12) Helgstrand, M.; Hard, T.; Allard, P. *J. Biomol. NMR* **2000**, *18*, 49-63.

(S13) Abragam, A. *The Principles of Nuclear Magnetic Resonance*, 1961, Clarendon Press, Oxford, England.

(S14) Lipari, G.; Szabo, A. *J. Am. Chem. Soc.* **1982**, *104*, 4546-4559.

(S15) Clore, G.M.; Szabo, A.; Bax, A.; Kay, L. E.; Driscoll, P. C.; Gronenborn, A. M. *J. Am. Chem. Soc.* **1990**, *112*, 4989-4991.

(S16) Clore, G. M.; Driscoll, P. C.; Gronenborn, A. M. *Biochemistry* **1990**, *29*, 7387-7401.

(S17) Alberty, R. A.; Hammes, G. G. *J. Phys. Chem.* **1958**, *62*, 154-159.

(S18) Avram, L.; Cohen, Y. *Chem. Soc. Rev.* **2015**, *44*, 586-602.

(S19) Freitas, C.; Müller, R.H. *Int. J. Pharmaceutics* **1998**, *168*, 221-229.

(S20) Vijay-Kumar, S.; Bugg, C. E.; Cook, W. J. *J. Mol. Biol.* **1987**, *194*, 531-544.

(S21) Schwieters, C. D.; Kuszewski, J.; Clore, G. M. *Progr. Nucl. Magn. Reson. Spectr.* **2006**, *48*, 47-62.